# Nanoelectromechanics using graphene

## Vibhor Singh[1,2,]* and Mandar M. Deshmukh[1]

[1]Department of Condensed Matter Physics and Materials Science, Tata Institute of Fundamental Research, Homi Bhabha Road, Mumbai 400 005, India
[2]Present address: Kavli Institute of Nanoscience, Delft University of Technology, Lorentzweg 1, 2628 CJ Delft, The Netherlands

**The large in-plane modulus of rigidity and low mass density of one-atom-thick graphene makes it an exciting material for studying mechanics at nanoscale. Further, the remarkable electronic properties of graphene give an additional edge to explore the small coupling between electronic and mechanical degrees of freedom. Ballistic transport can be reached in very clean suspended graphene samples, allowing to probe coupling between nanoscale electromechanics and quantum Hall effect. Such devices can also be used to measure intrinsic properties of graphene like coefficient of thermal expansion. In this article, we present summary of results from our group integrating these aspects of graphene. Towards the end, we briefly speculate roadmap for future experiments harnessing unique properties of graphene. Nanomechanical devices can then be used for applications as well as to explore aspects of mesoscopic physics with unprecedented detail.**

**Keywords:** Graphene, nanoelectromechanics, quantum Hall effect, thermal expansion.

## Introduction

ELECTRONIC properties of graphene[1] are of interest for fundamental science[2] as well as for applications since the first experiments probing quantum Hall effect (QHE)[3,4]. In addition to the electronic properties, the remarkable mechanical properties of graphene include a high in-plane Young's modulus of 1 TPa together with high fracture strength probed using nanoindentation of suspended graphene[5] and electromechanical resonators[6–9]. NEMS (nanoelectromechanical systems) devices using nanostructures such as carbon nanotubes[10–16], nanowires[17–19] and bulk micromachined structures[20–22] offer promise of new applications and allow us to probe fundamental properties at the nanoscale. NEMS-based devices are ideal platforms to harness the unique mechanical properties of graphene[23]. Electromechanical measurements with graphene resonators[7,8] suggest that with improvement of quality factor ($Q$), graphene-based NEMS devices have the potential to be sensitive detectors of mass and charge. Additionally, the sensitivity of graphene to chemical specific processes[3,24] offers the possibility of integrated mass and chemical detection. The large surface-to-mass ratio of graphene offers a distinct advantage over other nanostructures for such applications. As an example of the utility of suspended graphene devices, we show that such devices can be used to probe the coefficient of thermal expansion of graphene ($\alpha_{\text{graphene}}(T)$) as a function of temperature. These measurements indicate $\alpha_{\text{graphene}}(T)$ to be negative[25] for 30 K $< T <$ 300 K and larger in magnitude than theoretical prediction[26]. These experiments[25] also show that measuring temperature-dependent mechanical properties[27] of suspended structures down to low temperatures gives insight into strain engineering of graphene-based devices[28,29] and also helps in understanding the role of rippling in degrading carrier mobility at low temperatures. The other advantage which stems from these suspended resonators is the ability to clean them by applying large current. Such devices show very large carrier mobility, which can be used to study the ballistic transport, QHE at low magnetic fields and novel fractional quantum Hall states in high magnetic fields[30]. Realizing both the quantum Hall state and the ability to excite the vibrational modes leads us to ask the question – how do the vibrations affect the quantum Hall state and vice versa[31]. Later in the article, we answer this question in detail.

Several materials have been explored to probe the coupling between nanomechanics and electronic degrees[18,25,31–34]. However in this article, we focus on graphene nanomechanics. First we review the basics of QHE for graphene to set the stage for discussion of further experiments. Then, we take a slight detour to discuss details for the fabrication of suspended graphene and measurement schemes for the electromechanical actuation. Then, we give one example of the utility of the electromechanical measurements as the measurement of $\alpha_{\text{graphene}}$. After this we discuss another aspect of the suspended graphene devices, which is improvement of carrier mobility by current annealing, giving an example of the QHE in these systems.

## Quantum Hall effect in graphene

QHE is a quantum mechanical phenomenon that occurs in two-dimensional electronic systems subjected to magnetic field and is typically observable at low temperatures. In the presence of magnetic field, the current density ($\bar{J}$) no

longer remains parallel to the applied electric field ($\vec{E}$), ($\vec{J} = \sigma\vec{E}$), and hence conductance of the sample is described by $2 \times 2$ conductivity tensor with two independent components, namely longitudinal conductivity $\sigma_{xx}$ and transverse conductivity $\sigma_{xy}$. The localization–delocalization of electrons (for integer QHE) and electron–electron interactions (for fractional QHE) lead to versatile phenomena like dissipationless transport across the system and at the same time transverse conductance becomes quantized in units of $e^2/h$, irrespective of the details of material properties and sample geometry. A complete and detailed description of quantum Hall phenomenon is available in the literature[35–37].

A unique quantization sequence, of filling factors $v = \pm 2, \pm 6, \pm 10,\ldots$, is specific to monolayer graphene[3,4] and is often used to identify devices with monolayer graphene. In Figure 1 a, we show $R_{xx}$ and $R_{xy}$ with gate voltage at $T = 300$ mK and $B = 9$ T (ref. 38). At fixed field, the continuous density of states splits into highly degenerate discrete Landau levels. By changing the gate voltage, the Fermi energy can be moved across the Landau levels without modifying the energy spectrum. As gate voltage is swept vanishing longitudinal resistance, $R_{xx}$, and quantized plateaus in transverse resistance, $R_{xy}$, can be seen clearly. These filling factors correspond to monolayer graphene ($v = \pm 2$, $v = \pm 6$)[3,4]. As the magnetic field is changed, the position of Landau levels evolves given by $E_n = \pm\sqrt{2eB\hbar v_F n}$. In Figure 1 b, we plot the evolution of $R_{xy}$ as a function of $V_g$ and magnetic field $B$. As carrier density and magnetic field are changed, the integer filling factors evolve and get reflected in the form of a fan diagram shown in Figure 1 b. The plateaus in $R_{xy}$ corresponding to $v = \pm 2$, $\pm 6$ and $-10$ are clearly seen. The QHE is of interest not only from the perspective of fundamental nature of electronic excitations, but also from the point of view of meterology[39]. QHE provides the standard for resistance and efforts are ongoing to explore the suitability of graphene-based quantum Hall standards[40]. Another interesting aspect relevant to the experiments discussed here is the magnetization associated with the current-carrying states in quantum Hall limit. This magnetization leads to an additional spring constant in suspended graphene devices leading to a coupling between electron transport and mechanics, and will be discussed later in detail.

## Fabrication of suspended graphene devices

There are two key motivations for seeking to fabricate devices where graphene is suspended above the substrate – (a) to realize nanoscale electromechanical device to study the vibrational modes, and (b) to increase the mobility of the carriers in graphene.

In order to fabricate suspended graphene devices, one has to first make graphene – one-atom thick layer of

graphite. How does one isolate a monolayer of graphene and characterize it is a question that several researchers have spent a lot of time thinking about. Several different techniques have been developed to isolate graphene. The first one, known as the 'Scotch Tape' technique, is a method that Nobel laureates Andre Geim and Konstantin Novoselov used for their work. The second one is based on chemical vapour deposition (CVD) and utilizes the pyrolysis of methane over copper. We discuss briefly the Scotch Tape method.

The basic 'recipe' for making graphene using the 'Scotch Tape' technique requires the use of 300 nm $SiO_2$-coated silicon wafer as a substrate and cleaning it with a harsh etchant to remove any residue that it adhering to the wafer. Following this one patiently peels graphite by sandwiching it between the Scotch Tape repeatedly till the tape is translucent. Dabbing the tape on the $SiO_2$ wafer and peeling it off leads to deposition of an assortment of flakes of different thicknesses on the surface. Examining the surface with a simple optical microscope allows one to sift through the debris and locate the very thin flakes of graphene. Figure 2 shows an optical microscope image of such a deposition. One can clearly see that there are several flakes with differing colours. The thickest flake at the bottom of the image has silver colour, like a typical metal, is very thick ($\sim 500$ nm), whereas ones that have a dark blue colour are $\sim 50$ nm
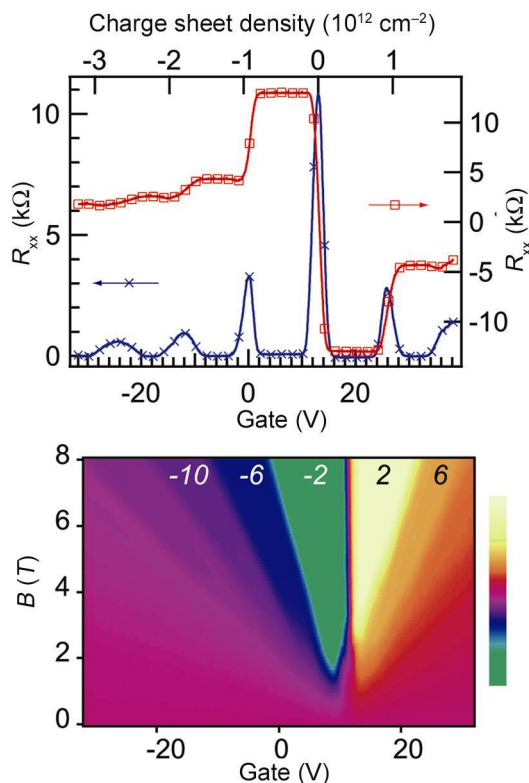


**Figure 1.** Plot of the longitudinal resistance ($R_{xx}$) and transverse resistance ($R_{xy}$) for a monolayer graphene device at 300 mK and 9 T. These measurements have also appeared in prior publication in ref. 38.

thick and the triangular flake that is barely visible is monolayer graphene.

To fabricate monolayer graphene electromechanical resonators, we suspend graphene devices using the previously reported process[8,41–43], which starts with micromechanical exfoliation of graphene from graphite crystal several millimetres thick onto a degenerately doped silicon wafer coated with 300 nm thick, thermally grown $SiO_2$. Following the location of monolayer graphene flakes using optical microscopy, electron beam lithography is used to pattern resist for fabricating electrodes for electrical contact. The electrodes are fabricated by evaporation of 10 nm of chromium and 60 nm of gold following patterning of resist. To release graphene from the $SiO_2$ substrate, a dilute buffered-HF solution is used to selectively etch an area around the graphene device by masking the rest of the substrate using polymer resist. Following a calibrated etch for 5 min 30 sec that results in a 150 nm deep trench in $SiO_2$, the device is rinsed in DI water and iso-propanol. Critical point drying, to prevent collapse of the device due to surface tension, is the final step in fabrication of suspended graphene devices. A scanning electron microscope (SEM) image of a suspended graphene device is shown in Figure 3 a. An interesting aspect of the suspended graphene devices is that the silicon oxide underneath the graphene buried under metallic electrodes is also etched. In effect, the gold electrodes are holding the freely suspended parts of graphene. This can be clearly seen in Figure 3 b, where the upper part of the electrodes and graphene have been removed by sonication. This aspect of partly suspended gold electrode (area overlapping with graphene) will become relevant in the experiments discussed in the following sections. Once the suspended devices are fabricated, they can be used for a variety of experiments.
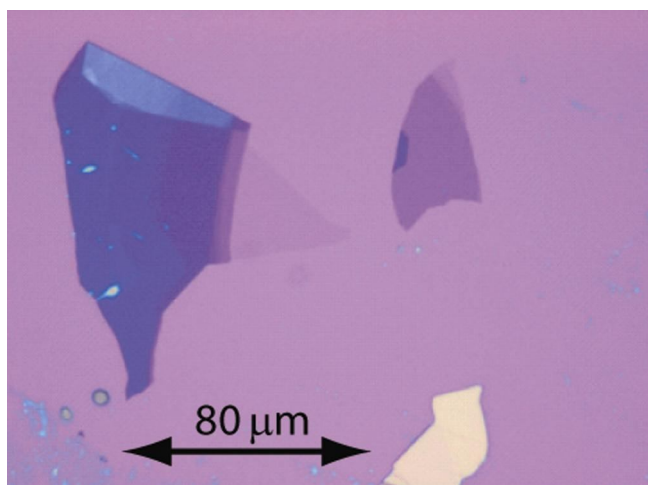
We would also like to point out that other variants of making suspended graphene devices have evolved as well, like the transfer of graphene on pre-patterned etch substrates. This can either be done using direct exfoliation from graphite[7] or from CVD graphene[44].

## Nanoelectromechanics using suspended graphene devices

A large field has developed over the last several decades studying NEMS; graphene has a lot to offer to this exciting area. An example of such a simple NEMS device is shown in Figure 3 a, which shows the SEM image of suspended graphene tethered to conducting posts and hanging 150 nm above the substrate. This device is similar to a mass attached to a spring, sitar, or a guitar, but a million times smaller (Figure 4 a). What is this useful for? Such NEMS devices are very sensitive detectors of mass and stress. How does a NEMS device measure mass? It is easy to understand the principle if one looks at the spring-mass system in Figure 4 a and monitors the resonant frequency; one can detect when the butterfly lands on it. The relative change in the resonant frequency $(\Delta f / f) \sim (\Delta m / m)$, where $\Delta m$ is the change in mass and $m$ is the mass of the resonator. To get maximum sensitivity, implying large $\Delta f / f$, one would really like a small $m$ so
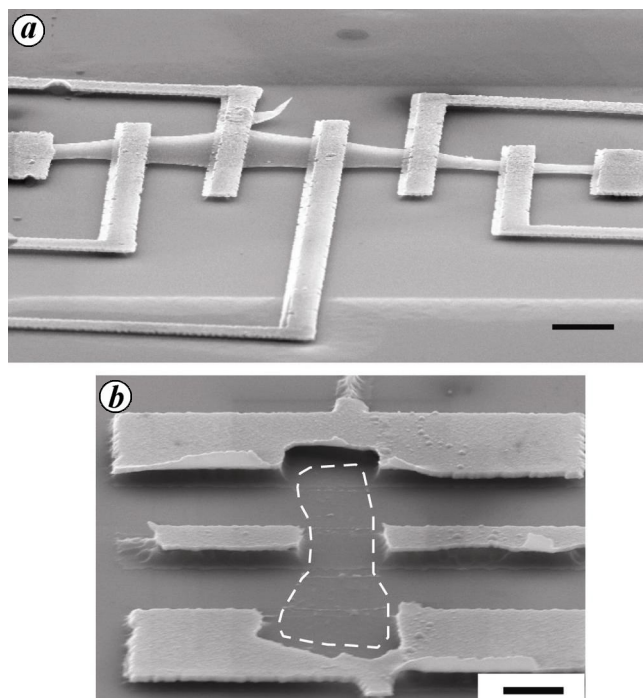


**Figure 3.** *a*, Tilted scanning electron microscopic (SEM) image of a suspended graphene flake connected with multiple electrodes held ~ 150 nm above the substrate. Scale bar corresponds to 2 μm. *b*, Tilted SEM image of a suspended graphene device after removal of the graphene flake. The dashed outline shows the original position of the graphene flake. The scale bar corresponds to 1 μm.



**Figure 2.** An optical microscope image of graphene after peeling using the 'Scotch Tape' technique. The 300 nm thick $SiO_2$-coated Si wafer has a purple colour and the colour changes subtly where layers of graphene are deposited. The triangular flap of monolayer graphene is clearly seen. Other flakes of graphene show varying colour.

that even a small additional mass $\Delta m$ leads to large change in frequency. This sensitivity is the main reason why resonators based on graphene are desirable – they offer very low mass density and the ability to detect small molecules.

Nanoelectromechanical devices, much like stringed instruments, have two important components associated with them: (a) actuation, akin to plucking, and (b) detection, where one listens to the notes emanating from the stringed instrument. Both these aspects are embedded in our device. Actuation of the device is done by capacitive means with graphene forming one electrode of a parallel plate capacitor. The detection relies on the crucial fact that as the graphene membrane vibrates in one part of the cycle, it moves closer to the gate electrode and in the other moves away from the gate. As graphene has a finite transconductance, the motion relative to the gate results in modulation of the graphene membrane conductance. This conductance modulation is largest at the electro-

mechanical resonance where the amplitude of mechanical motion is maximal. So, measuring the modulation of the conductance as a function of the actuation frequency will allow one to measure the electromechanical resonance. However, the measurement of conductance modulation by simply biasing is challenging as the parasitic capacitance leads to generation of displacement current at actuation frequency. As a result, one needs to use a different method to measure the resulting modulation in conductance.

We discuss the details of the technique next. The electrical actuation and detection are done using the suspended graphene device as heterodyne-mixer[8,12,16]. The scheme for electrical actuation and detection is shown in Figure 4 b, superimposed on the SEM image of the device. The electrostatic interaction between the graphene membrane and the back-gate electrode is used to actuate the motion in a plane perpendicular to the substrate. A radio frequency (RF) signal $V_g(\omega)$ and a DC voltage $V_g^{DC}$ are applied at the gate terminal using a bias-tee. Another RF signal $V_{SD}(\omega + \Delta\omega)$ is applied to the source electrode (Figure 4 b). RF signal applied at the gate $V_g(\omega)$ modulates the gap between graphene and the substrate at frequency $\omega$, and $V_g^{DC}$ alters the overall tension and carrier density in the membrane. The amplitude of the current through the graphene membrane at the difference frequency ($\Delta\omega$), also called the mixing current $I_{mix}(\Delta\Omega)$, can be written as[8,11,12,14,16,45]:

$$I_{mix}(\Delta\omega) = \frac{1}{2}\frac{dG}{dq}\left(\frac{dC_g}{dz}z(\omega)V_g^{DC} + C_g V_g(\omega)\right)$$
$$\times V_{SD}(\omega + \Delta\omega), \tag{1}$$

where $G$ is the conductance of the graphene device, $q$ the charge induced by the gate voltage, $C_g$ the capacitance between the gate electrode and graphene and $z(\omega)$ is the amplitude of oscillation at the driving frequency $\omega$ along the $z$-axis (perpendicular to the substrate). The difference frequency signal (at $\Delta\omega$) arises from the product of the modulation signals of $V_{SD}(\omega + \Delta\omega)$ and $G(\omega)$. At the mechanical resonance of the membrane, the first term in eq. (1) contributes significantly and the second term, which does not depend on the mechanical motion of the graphene membrane, provides a smooth background.

Figure 4 c shows the result of such a measurement at 7 K for a suspended graphene device while $V_g^{DC}$ is set at –5 V. Using a modified Lorentzian lineshape for the resonance curve[12,46], we can extract the quality factor $Q = 1500$ of the resonator. Figure 4 d shows the colour-scale plot of $I_{mix}(\Delta\Omega)$ as a function of $V_g^{DC}$ and $f = \omega/2\pi$ at 300 K. The resonant frequency increases as the magnitude of $V_g^{DC}$ is increased – mechanical mode disperses positively with $V_g^{DC}$. This is well understood in terms of increase in the tension of the graphene resonator, due to electrostatic attraction between the membrane and back
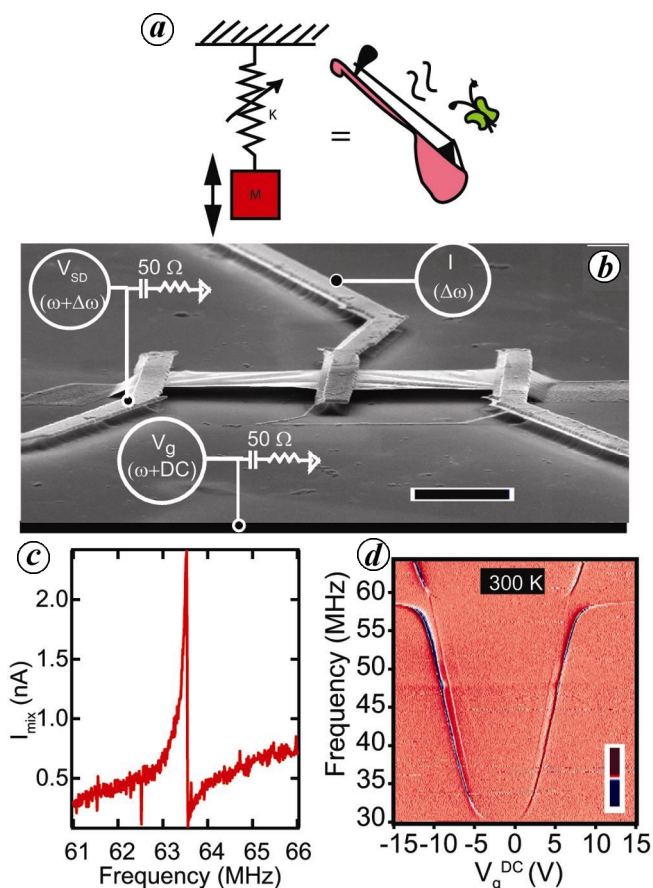
**Figure 4.** *a*, The equivalence between various resonant systems like mass attached to a spring and a percussion instrument. *b*, Tilted angle SEM image of a suspended monolayer graphene device and the electrical circuit for actuation and detection of the mechanical motion of the graphene membrane. Scale bar indicates a length of 2 μm. *c*, Plot of the mixing current $I_{mix}(\Delta\omega)$ as a function of frequency *f*. The sharp feature in the mixing current corresponds to the mechanical resonance. *d*, Colourscale plot of the mixing current as a function of frequency *f* and DC gate voltage $V_g^{DC}$ at 300 K.

gate, as the gate voltage is increased. The physics here is similar to the change in frequency of the sound that comes from a guitar string as the musician tightens the peg holding the string.

## Utilizing graphene NEMS to measure thermal expansion of graphene

The resonant frequency $f_0$ of the graphene membrane is a measure of strain in the flake and in tensile limit can be approximated as:

$$f_0(V_g^{DC}) = \frac{1}{2L}\sqrt{\frac{\Gamma(\Gamma_0(T), V_g^{DC}}{\rho tw}}, \qquad (2)$$

where $L$ is the length of the membrane, $w$ the width, $t$ the thickness, $\rho$ the mass density, $\Gamma_0(T)$ the in-built tension
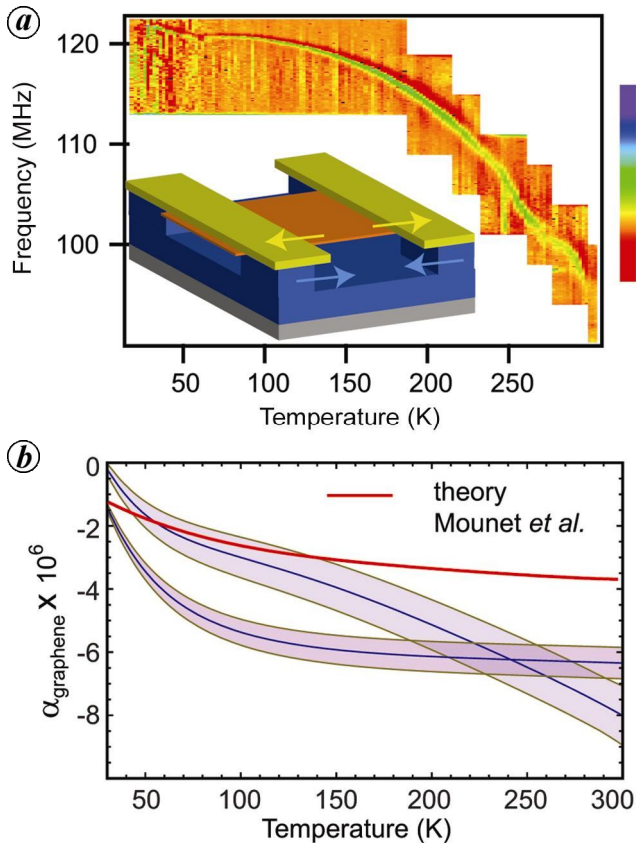
**Figure 5.** *a*, Plot showing the evolution of resonant frequency of a mode for a device as a function of temperature for $V_g^{DC} = 15$ V. (Inset) Schematic of all the strains external to the suspended graphene membrane as the device is cooled below 300 K. *b*, Plot of expansion coefficient of graphene as a function of temperature. Data from two different devices together with theoretical prediction of Mounet and Marzari[26]. The shaded area represents the errors estimated from the uncertainty of the length of the flake, width of the electrode and Young's modulus of graphene. These measurements have also appeared in prior publication in ref. 25.

and $\Gamma$ is the tension at a given temperature $T$ and $V_g^{DC}$. The functional form of $\Gamma(\Gamma_0(T), V_g^{DC})$ is dependent on details of the model used to take into account the electrostatic and elastic energies.

We now consider how the resonant frequency ($f_0$) evolves as a function of temperature. Figure 5 *a* shows the result of an evolution of a mode as a function of temperature at $V_g^{DC} = 15$ V. This increase has been seen in all the devices we have studied. The degree of frequency shift varies from one device to another depending on the device geometry. The origin of this frequency shift with temperature is the increase in tension in graphene due to the expansion/contraction of substrate, gold electrodes and graphene. The frequency shift can be understood by taking into account the contribution of various strains as the device is cooled below 300 K. The three main contributions are – first, the thermal strain in unconstrained graphene $\varepsilon_{graphene}(T) = \int_T^{300} \alpha_{graphene}(t)dt$ due to the coefficient of thermal expansion of graphene $\alpha_{graphene}(T)$; second, the thermal strain due to the gold electrodes $\varepsilon_{gold}(T) = \int_T^{300} \alpha_{gold}(t)dt$, and lastly, the contribution of the strain induced by the substrate $\varepsilon_{substrate}(T)$; here $\varepsilon_{gold}(T)$ is the coefficient of thermal expansion for gold[47]. The strain in gold electrodes plays an important role due to the geometry of the device. As mentioned earlier and seen in Figure 3 *b*, the under-etch that releases the graphene membrane also etches under the graphene covered by the electrodes – resulting in the graphene membrane being suspended off the gold electrodes[8]. The geometry of the resulting device is shown in the inset to Figure 5 *a*. The elastic strain in the curved substrate can be calculated using Stoney's equation[48]. Its contribution to the net strain in the graphene membrane is very small and therefore upon cooling, change of tension in the graphene is due to contraction of gold electrode and expansion/contraction of graphene. We assume that the Young's modulus of graphene does not vary significantly over the temperature range[49]. At the interface of gold electrodes supporting the graphene membrane, the net force must balance to zero; however, the stresses are different considering the cross-sectional area of gold electrodes (~500 nm × 60 nm) and graphene (~ 500 nm × 0.3 nm). The large difference in the cross-sectional area implies that the effective stiffness of gold electrodes is large compared to the stiffness of graphene. As a result, to a very good approximation, the total elastic strain at a given temperature in graphene that is confined by 'rigid' gold electrodes is $\varepsilon_{grapheneclamped} = \varepsilon_{graphene}(T) + \varepsilon_{substrate}(T) - \varepsilon_{gold}(T)\frac{w_{electrode}}{L}$, where $w_{electrode}$ is the average of the width of gold electrodes holding the suspended flake. The change in tension in the membrane can be written as a function of temperature as $\Delta\Gamma_0(T) = wt\varepsilon_{grapheneclamped}(T)E_{graphene}$, where $E_{graphene}$ is the Young's modulus of graphene. Measuring the tension $\Gamma_0(T)$ as a function of temperature offers a way to track the thermal strain in graphene membrane. Figure 5 *a* shows the

evolution of resonant frequency as a function of temperature from a device at $V_g^{DC} = 15$ V, where the increase in frequency is largely due to the contraction of the gold electrodes. However, this rate of increase of resonant frequency is significantly reduced due to the negative $\alpha_{graphene}$ for all $T < 300$ K from the case of frequency change, including only the contraction of gold. Using such a measurement of frequency shift while assuming uniform expansion of all the materials and using eq. (2), it is possible to calculate the expansion coefficient from the frequency at $V_g^{DC} = 0$ V as

$$\alpha_{graphene}(T) = -2f_0(0)\frac{df_0(0)}{dT} \times \frac{(2L)^2 \rho}{E_{graphene}}$$

$$+ \frac{d}{dT}\left(\varepsilon_{substrate}(T) - \varepsilon_{gold}(T)\frac{w_{electrode}}{L}\right). \quad (3)$$

Figure 5 b shows the result of calculating $\alpha_{graphene}$ for two devices using this analysis and comparison with the theoretical calculation for $\alpha_{graphene}$ by Mounet and Marzari[26]. We find that $\alpha_{graphene}$ is negative and its magnitude decreases with temperature for $T < 300$ K. At room temperature, $\alpha_{graphene} \sim -7 \times 10^{-6}$ K$^{-1}$, which is similar to the previously reported values measured by others[8,50]. At 30 K, $\alpha_{graphene} \sim -1 \times 10^{-6}$ K$^{-1}$. The deviation of $\alpha_{graphene}$ from the theoretically predicted values can possibly be due to the presence of the impurities on graphene membrane. The knowledge of $\alpha_{graphene}$ is essential for the fabrication of the devices intended for strain engineering applications[28,29]. Strain engineering of graphene devices at low temperatures using this picture can improve device performance, for example, by enabling temperature compensation[51] or achieving high strain for large frequency and low phonon occupancy.

## High-mobility suspended graphene to study quantum Hall effect

We now discuss how these suspended graphene devices can have very high mobility as the scattering due to the dangling bonds and other dopants on the surface of SiO$_2$ trapped beneath graphene is eliminated. The procedure for fabricating the suspended graphene has been already described earlier.

Figure 6 a shows the variation of zero bias conductance of graphene device with gate voltage right after fabrication (top curve). The device after fabrication has no clear Dirac peak (the charge neutrality point) and poor charge carrier mobility. To improve its performance, the device is annealed at cryogenic temperatures in cryogenic vacuum by injecting gradually larger current through it (Figure 6 b)[8,25,41–43] and switching the polarity after some changes in conductance are observed. Current annealing increases the local temperature and ablates the resist

residue and organic traces due to various lithographic steps. Figure 6 a shows the result of various repetitions of current annealing procedure on the same device and gradually one observes a sharp Dirac peak as a function of gate voltage. To optimize the cleaning process, the gate response is checked after every cleaning step. At the end of the last annealing step, the mobility of the suspended device is in the excess of 150,000 cm$^2$ V$^{-1}$ s$^{-1}$. Similar mobilities have been observed by other groups[8,25,41–43].

The high mobility of the current annealed device (Figure 7 a) also reflects into the observation of integer quantum Hall effect (IQHE) at very low magnetic fields as the disorder is significantly reduced. Figure 7 b shows the robust integer quantum Hall plateaus seen at 5 K and magnetic fields less than 8 T; this is due to the low disorder within the suspended graphene membrane.

In one part of our experiment we probe the response of the quantum Hall state at resonant actuation. For this, we measure the DC resistance of the device while driving it through resonant frequency, by applying an RF signal at the gate electrode. The resonant frequency of the device
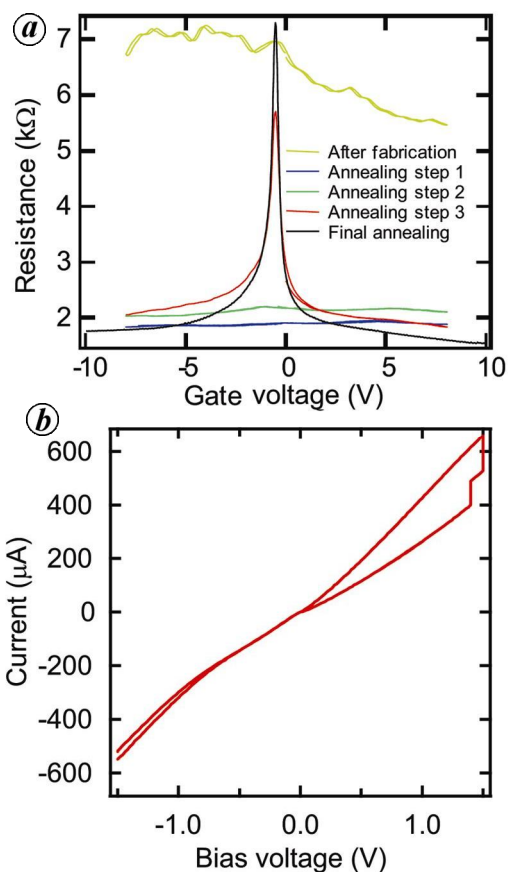


**Figure 6.** *a*, Current annealing of the graphene device by passing bipolar current. Initially the graphene device does not show the Dirac peak and has overall high resistance. *b*, Plot of current and voltage as the suspended graphene device is biased. The abrupt jumps at the extreme voltage bias indicate resistance changes in the device.
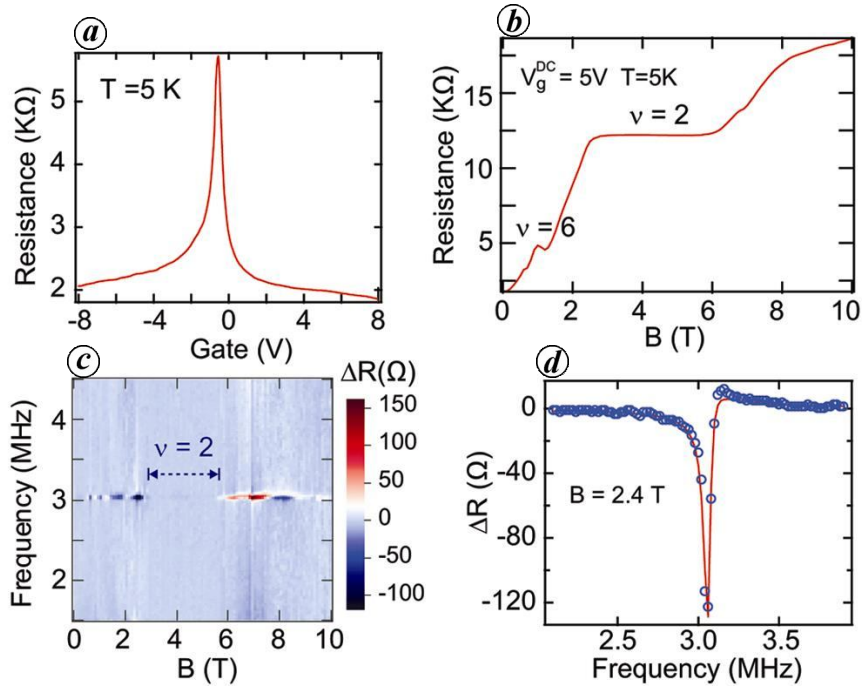
**Figure 7.** *a*, Two-probe device resistance as a function of gate voltage. The sharp Dirac peak due to current annealing is evident. The mobility of the device ~ 100,000 cm$^2$/Vs. *b*, Resistance as a function of magnetic field at $V_g^{DC} = 5$ V. *c*, Colourscale plot of the change in resistance ($\Delta R$) with magnetic field and driving frequency. The resonant frequency of the mode is 3.05 MHz. *d*, $\Delta R$ plotted with driving frequency along with the fitted curve. These measurements have also appeared in prior publication in ref. 31.

can be measured using mixing technique prior to these measurements. We define change in resistance ($\Delta R$) by subtracting the device resistance measured away from the resonant frequency ($R_0(B)$) from the device resistance ($\Delta R(B) = R(B) - R_0(B)$). Figure 7 *c* shows $\Delta R$ as a function of driving frequency and magnetic field. Some features can be clearly observed: (a) $\Delta R$ is zero in the plateau region, (b) $\Delta R$ has different signs across the quantum Hall plateaus, and (c) $\Delta R$ oscillates with $B$ for low values of magnetic field. Figure 7 *d* shows a slice of the data as a function of frequency and $\Delta R$ shows a Fano line shape. Such a behaviour in $\Delta R(B)$ can be understood by combining effects of graphene mechanics to QHE. The driving voltage ($V_{ac}$) applied at the gate terminal not only sets the motion ($z$-direction) in the flake at resonance frequency but also changes the carrier density due to finite capacitance ($C_0$) between the flake and the gate. Across resonance ($\omega \sim \omega_0$), the driving signal and motion of the flake can have a phase difference. Combining this electromechanics to the nonlinear dependence of magneto-resistance with magnetic field in the quantum Hall regime gives a Fano line shape to $\Delta R$ and is given by[31]

$$\Delta R = \frac{d^2 R}{dV_g^{DC2}} \left( \frac{(\tilde{\omega} + q_x)^2 + q_y^2}{\tilde{\omega}^2 + 1} - 1 \right) (V_{ac}^2),$$

where

$$q_x = -\left( \frac{1}{C_0} \frac{dC}{dz} \right) \left( V_g^{DC} \frac{dF}{dV} \right) \left( \frac{Q}{m\omega_0^2} \right), \quad \tilde{\omega} = \frac{\omega - \omega_0}{\gamma / 2}$$

and $q_y = 1$.

Figure 7 *d* shows experimentally measured $\Delta R$ along with fitted curve based on eq. (4).

Having considered the effect of electromechanics of graphene on QHE, we now look at the converse of it, i.e. how does quantum Hall state affect the electromechanics of graphene? In Figure 8 *a*, we have shown $I_{mix}$ for two modes, using frequency modulation technique[52], with magnetic field. The colourscale plot shows that two modes have different dispersion with magnetic field. In Figure 8 *b*, the non-monotonic resonant frequency shift ($\Delta f = f_0(B) - f_0(0)$) with $B$ can be seen for the two modes. At low magnetic fields, for the upper mode (115.77 MHz) $\Delta f$ increases with $B$ accompanied by a reduction in $Q$ (green colour shaded area in Figure 8 *b* and *c*). At the $\nu = 2$ plateau, $I_{mix}$ signal becomes very small ($dG/dV_g^{DC} \sim 0$) and the estimation of $f_0$ and $Q$ becomes difficult. As $B$ is increased further, after the $\nu = 2$ plateau, $\Delta f$ starts dropping slowly without much change in $Q$ (yellow colour shaded area in Figure 8 *b* and *c*). Similar behaviour can be seen for the lower frequency mode (115.124 MHz), though the effect is less pronounced (Figure 8 *d*).
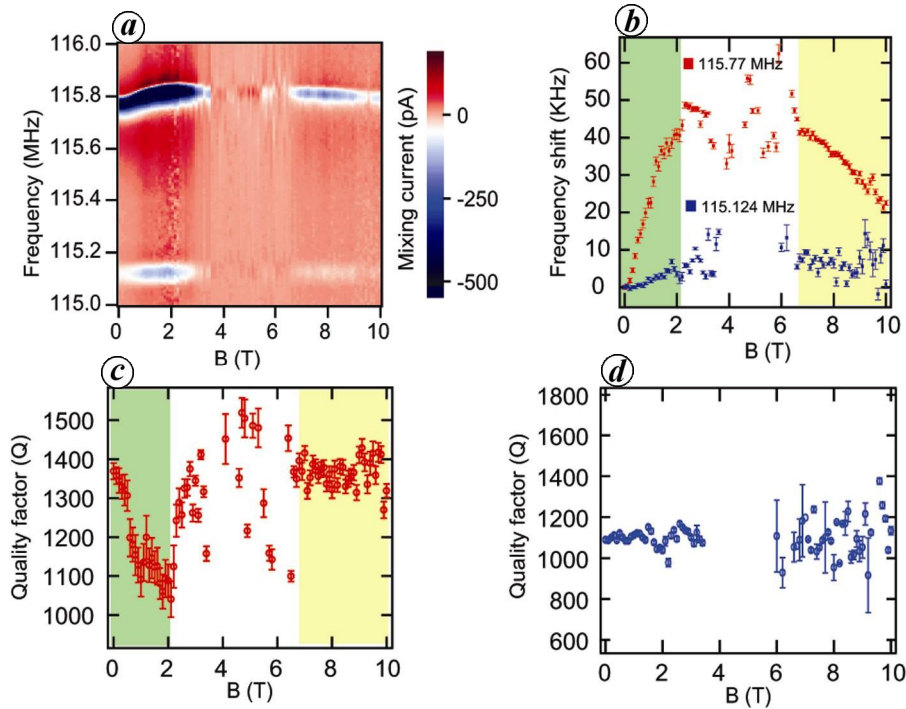
**Figure 8.** Resonant frequency and quality factor with magnetic field (*B*) at 5 K and $V_g^{DC}$ = 5 V. *a*, Measurement of mixing current for two closeby mechanical modes with *B*. *b*, Frequency shift with *B* by fitting the data in (*a*). Different behaviour in frequency shift across the $\nu$ = 2 plateau is shown with shaded region. *c*, *d*, Variation of the quality factor with *B* for the two modes shown in (*a*) at frequencies 115.77 and 115.124 MHz respectively. These measurements have also appeared in prior publication in ref. 31.
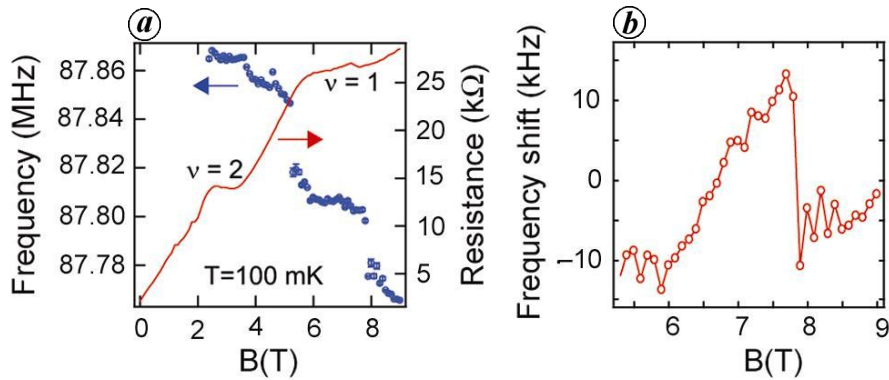


**Figure 9.** *a*, Measurement of resistance and resonant frequency at *T* = 100 mK and $V_g^{DC}$ = 3 V. *b*, Frequency shift after removing a smooth parabolic background of frequency from the data shown in (*a*).

Such an effect on the electromechanics of graphene (resonant frequency and quality factor of the resonator) due to quantum Hall state can be understood by considering all the contributions to the total energy of the resonator. The quantum Hall state contributes to this energy due to finite magnetization (*M*) originating from localized and delocalized states and is given by $-M \cdot B$. However, at resonance, as graphene vibrates electron density in the flake also oscillates, which leads to an implicit dependence of magnetization (*M*) on the position of the flake (*z*)

and hence provides a coupling to electromechanics. Since this coupling relies on the fractional changes in carrier density at resonance, it makes the observed effects on electromechanics mode dependent, reflecting the fact that different resonant modes have different spatial profiles and hence different coupling.

The advantage of cleaning suspended graphene samples allows one to observe broken symmetry states at easily accessible magnetic field and temperature. In Figure 9 *a*, we show the variation in resistance and resonant

frequency of a device with magnetic field. In resistance, the plateau at $\nu = 2$ and $\nu = 1$ can be clearly seen. $\nu = 1$ originates from the interaction-induced broken symmetries of zeroth Landau level. Effect of such broken symmetry states can also be seen on electromechanics of graphene. However, a detailed understanding of such an effect goes beyond our simple model based on the magnetization of the quantum Hall state. If a smooth parabolic fitted background of frequency is subtracted, jumps in resonant frequency can be accentuated as shown in Figure 9 b. The origin of such an overall background of frequency could arise from any paramagnetic ions present on graphene[53]. Such coupling between the electronic states and the mechanics offers a means to probe aspects of physical problems in a unique way.

## Summary

In this article, we mainly discussed our efforts toward harnessing graphene electromechanics to study its intrinsic properties and exploring its coupling to electronic degrees of freedom. However, graphene has much more to offer. Unique combination of low mass, high stiffness and large surface area can be utilized make high-frequency resonators for sensing applications. Coupling of these mechanical resonators to superconducting circuits can be used to study quantum effects like cooling to ground state, decoherence of mechanical states in these structure and using them as an active element of quantum memory. Utilizing negative thermal expansion coefficient of graphene, a high-frequency strain-engineered resonator can be fabricated, which can be easily cooled to ground state at dilution fridge temperatures.

1. Castro Neto, A. H., Guinea, F., Peres, N. M. R., Novoselov, K. S. and Geim, A. K., The electronic properties of graphene. *Rev. Mod. Phys.*, 2009, **81**, 109–162; http://link.aps.org/doi/10.1103/RevModPhys.81.109

2. Novoselov, K. S. *et al.*, Electric field effect in atomically thin carbon films. *Science*, 2004, **306**(5696), 666–669.

3. Novoselov, K. S. *et al.*, Two-dimensional gas of massless dirac fermions in graphene. *Nature*, 2005, **438**, 197–200; ISSN 0028-0836, http://dx.doi.org/10.1038/nature04233

4. Zhang, Y., Tan, Y., Stormer, H. L. and Kim, P., Experimental observation of the quantum hall effect and berry's phase in graphene. *Nature*, 2005, **438**, 201–204; ISSN 0028-0836, http://dx.doi.org/10.1038/nature04235

5. Lee, C., Wei, X., Kysar, J. W. and Hone, J., Measurement of the elastic properties and intrinsic strength of monolayer graphene. *Science*, 2008, **321**(5887), 385–388.

6. Chen, C. and Hone, J., Graphene nanoelectromechanical systems. *Proceedings IEEE*, 2013, **101**(7), 1766–1779, ISSN 0018-9219.

7. Bunch, J. S. *et al.*, Electromechanical resonators from graphene sheets. *Science*, 2007, **315**(5811), 490–493.

8. Chen, C. *et al.*, Performance of monolayer graphene nanomechanical resonators with electrical readout. *Nat. Nanotechnol.*, 2009, **4**, 861–867.

9. Garcia-Sanchez, D., van der Zande, A. M., Paulo, A. S., Lassagne, B., McEuen, P. L. and Bachtold, A., Imaging mechanical vibrations in suspended graphene sheets. *Nano Lett.*, 2008, **8**(5), 1399–1403.

10. Huttel, A. K., Steele, G. A., Witkamp, B., Poot, M., Kouwenhoven, L. P. and van der Zant, H. S. J., Carbon nanotubes as ultrahigh quality factor mechanical resonators. *Nano Lett.*, 2009, **9**(7), 2547–2552.

11. Lassagne, B., Tarakanov, Y., Kinaret, J., Garcia-Sanchez, D. and Bachtold, A., Coupling mechanics to charge transport in carbon nanotube mechanical resonators. *Science*, 2009, **325**(5944), 1107–1110.

12. Sazonova, V., Yaish, Y., Ustunel, H., Roundy, D., Arias, T. A. and McEuen, P. L., A tunable carbon nanotube electromechanical oscillator. *Nature*, 2004, **431**(7006), 284–287.

13. Steele, G. A., Huttel, A. K., Witkamp, B., Poot, M., Meerwaldt, H. B., Kouwenhoven, L. P. and van der Zant, H. S. J., Strong coupling between single-electron tunneling and nanomechanical motion. *Science*, 2009, **325**(5944), 1103–1107.

14. Chiu, H.-Y., Hung, P., Postma, H. W. C. and Bockrath, M., Atomic-scale mass sensing using carbon nanotube resonators. *Nano Lett.*, 2008, **8**(12), 4342–4346.

15. Knobel, R., Yung, C. S. and Cleland, A. N., Single-electron transistor as a radio-frequency mixer. *Appl. Phys. Lett.*, 2002, **81**(3), 532–534.

16. Lassagne, B., Garcia-Sanchez, D., Aguasca, A. and Bachtold, A., Ultrasensitive mass sensing with a nanotube electromechanical resonator. *Nano Lett.*, 2008, **8**(11), 3735–3738.

17. Feng, X. L., He, R., Yang, P. and Roukes, M. L., Very high frequency silicon nanowire electromechanical resonators. *Nano Lett.*, 2007, **7**(7), 1953–1959.

18. Solanki, H. S. *et al.*, Tuning mechanical modes and influence of charge screening in nanowire resonators. *Phys. Rev. B*, 2010, **81**(11).

19. He, R., Feng, X. L., Roukes, M. L. and Yang, P., Self-transducing silicon nanowire electromechanical systems at room temperature. *Nano Lett.*, 2008, **8**(6), 1756–1761; http://pubs.acs.org/doi/abs/10.1021/nl801071w

20. Carr, D. W., Evoy, S., Sekaric, L., Craighead, H. G. and Parpia, J. M., Measurement of mechanical resonance and losses in nanometer scale silicon wires. *Appl. Phys. Lett.*, 1999, **75**(7), 920–922.

21. Naik, A. K., Hanay, M. S., Hiebert, W. K., Feng, X. L. and Roukes, M. L., Towards single-molecule nanomechanical mass spectrometry. *Nature Nanotechnol.*, 2009, **4**(7), 445–450.

22. Unterreithmeier, Q. P., Weig, E. M. and Kotthaus, J. P., Universal transduction scheme for nanomechanical systems based on dielectric forces. *Nature*, 2009, **458**(7241), 1001–1004.

23. Ekinci, K. L. and Roukes, M. L., Nanoelectromechanical systems. *Rev. Sci. Instrum.*, 2005, **76**(6), 061101–061112.

24. Schedin, F., Geim, A. K., Morozov, S. V., Hill, E. W., Blake, P., Katsnelson, M. I. and Novoselov, K. S., Detection of individual gas molecules adsorbed on graphene. *Nature Mater.*, 2007, **6**(9), 652–655.

25. Singh, V. *et al.*, Probing thermal expansion of graphene and modal dispersion at low-temperature using graphene nanoelectromechanical systems resonators. *Nanotechnology*, 2010, **21**, 165204.

26. Mounet, N. and Marzari, N., First-principles determination of the structural, vibrational and thermodynamic properties of diamond, graphite, and derivatives. *Phys. Rev. B*, 2005, **71**(20), 205214.

27. Bao, W., Miao, F., Chen, Z., Zhang, H., Jang, W., Dames, C. and Lau, C. N., Controlled ripple texturing of suspended graphene and ultrathin graphite membranes. *Nature Nanotechnol.*, 2009, **4**(9), 562–566, ISSN 1748-3387, http://dx.doi.org/10.1038/nnano.2009.191

28. Pereira, V. M. and Neto, A. H. C., Strain engineering of graphene's electronic structure. *Phys. Rev. Lett.*, 2009, **103**(4), 046801–046804.

29. Guinea, F., Katsnelson, M. I. and Geim, A. K., Energy gaps and a zero-field quantum hall effect in graphene by strain engineering. *Nature Phys.*, 2010, **6**, 30–33.

30. Bolotin, K. I., Ghahari, F., Shulman, M. D., Stormer, H. L. and Kim, P., Observation of the fractional quantum hall effect in graphene. *Nature*, 2009, **462**, 196–199; ISSN 0028-0836, http://www.nature.com/nature/journal/v462/n7270/full/nature08582.html

31. Singh, V. *et al.*, Coupling between quantum hall state and electromechanics in suspended graphene resonator. *Appl. Phys. Lett.*, 2012, **100**(23), 233103; http://link.aip.org/link/?APL/100/233103/1.

32. Solanki, H. S. *et al.*, High Q electromechanics with InAs nanowire quantum dots. *Appl. Phys. Lett.*, 2011, **99**(21), 213104; http://link.aip.org/link/?APL/99/213104/1

33. Sengupta, S., Solanki, H. S., Singh, V., Dhara, S. and Deshmukh, M. M., Electromechanical resonators as probes of the charge density wave transition at the nanoscale in NbSe$_2$. *Phys. Rev. B*, 2010, **82**, 155432; http://link.aps.org/doi/10.1103/PhysRevB.82.155432

34. Sengupta, S., Samudrala, N., Singh, V., Thamizhavel, A., Littlewood, P. B., Tripathi, V. and Deshmukh, M. M., Plasmon mode modifies the elastic response of a nanoscale charge density wave system. *Phys. Rev. Lett.*, 2013, **110**, 166403; http://link.aps.org/doi/10.1103/PhysRevLett.110.166403

35. Prange, R. and Girvin, S. M., *The Quantum Hall Effect*, Springer Verlag, New York, 1990.

36. Sarma, S. and Pinczuk, A., *Perspectives in Quantum Hall Effects: Novel Quantum Liquids in Low-Dimensional Semiconductor Structures*, Wiley-VCH, Weinheim, Germany, 2004.

37. Yennie, D. R., Integral quantum Hall effect for nonspecialists. *Rev. Mod. Phys.*, 1987, **59**, 781–824; http://link.aps.org/doi/10.1103/RevModPhys.59.781

38. Singh, V. and Deshmukh, M. M., Nonequilibrium breakdown of quantum hall state in graphene. *Phys. Rev. B*, 2009, **80**, 081404; http://link.aps.org/doi/10.1103/PhysRevB.80.081404

39. Novoselov, K. S. *et al.*, Room-temperature quantum hall effect in graphene. *Science*, 2007, **315**(5817), 1379.

40. Giesbers, A. J. M. *et al.*, Quantum resistance metrology in graphene. *Appl. Phys. Lett.*, 2008, **93**(22), 222109–222109-3; ISSN 0003-6951.

41. Bolotin, K. I., Sikes, K. J., Hone, J., Stormer, H. L. and Kim, P., Temperature-dependent transport in suspended graphene. *Phys. Rev. Lett.*, 2008, **101**, 096802; http://link.aps.org/doi/10.1103/PhysRevLett.101.096802

42. Bolotin, K. I. *et al.*, Ultrahigh electron mobility in suspended graphene. *Solid State Commun.*, 2008, **146**(9–10), 351–355.

43. Du, X., Skachko, I., Barker, A. and Andrei, E. Y., Approaching ballistic transport in suspended graphene. *Nature Nanotechnol.*, 2008, **3**(8), 491–495.

44. Barton, R. A., Ilic, B., van der Zande, A. M., Whitney, W. S., McEuen, P. L., Parpia, J. M. and Craighead, H. G., High, size-dependent quality factor in an array of graphene mechanical resonators. *Nano Lett.*, 2011, **11**(3), 1232–1236; http://pubs.acs.org/doi/pdf/10.1021/nl1042227, http://pubs.acs.org/doi/abs/10.1021/nl1042227

45. Jensen, K., Kim, K. and Zettl, A., An atomic-resolution nanomechanical mass sensor. *Nature Nanotechnol.*, 2008, **3**(9), 533–537; ISSN 1748-3387, http://dx.doi.org/10.1038/nnano.2008.200

46. Sazonova, V., A tunable carbon nanotube resonator, Ph D thesis, Cornell University, USA, 2006.

47. Nix, F. C. and MacNair, D., The thermal expansion of pure metals: Copper, gold, aluminum, nickel, and iron. *Phys. Rev.*, 1941, **60**(8), 597.

48. Freund, L. B. and Suresh, S. (eds), *Thin Film Materials*, Cambridge University Press, 2003; ISBN: 9780521822817.

49. Jiang, J.-W., Wang, J.-S. and Li, B., Young's modulus of graphene: A molecular dynamics study. *Phys. Rev. B*, 2009, **80**(11), 113404–113405.

50. Bao, W., Miao, F., Chen, Z., Zhang, H., Jang, W., Dames, C. and Lau, C. N., Controlled ripple texturing of suspended graphene and ultrathin graphite membranes. *Nature Nanotechnol.*, 2009, **4**, 562–566.

51. Ho, G. K., Sundaresan, K., Pourkamali, S. and Ayazi, F., Low-motional-impedance highlytunable I$^2$ resonators for temperature-compensated reference oscillators. In MEMS 2005, 18th IEEE International Conference, FL, USA, 2005, pp. 116–120.

52. Gouttenoire, V., Barois, T., Perisanu, S., Leclercq, J.-L., Purcell, S. T., Vincent, P. and Ayari, A., Digital and FM demodulation of a doubly clamped single-walled carbon-nanotube oscillator: Towards a nanotube cell phone. *Small*, 2010, **6**(9), 1060–1065; ISSN 1613-6829, http://dx.doi.org/10.1002/smll.200901984

53. Harris, J. G. E., Knobel, R., Maranowski, K. D., Gossard, A. C., Samarth, N. and Awschalom, D. D., Magnetization measurements of magnetic two-dimensional electron gases. *Phys. Rev. Lett.*, 2001, **86**, 4644–4647; http://link.aps.org/doi/10.1103/PhysRevLett.86.4644